Corrosion Resistance of Multilayer Coatings Deposited by PVD on Inconel 718 Using Electrochemical Impedance Spectroscopy Technique

Citlalli Gaona-Tiburcio [1], Marvin Montoya-Rangel [1], José A. Cabral-Miramontes [1], Francisco Estupiñan-López [1], Patricia Zambrano-Robledo [1], Ricardo Orozco Cruz [2], José G. Chacón-Nava [3], Miguel Ángel Baltazar-Zamora [4] and Facundo Almeraya-Calderón [1,*]

[1] Universidad Autonoma de Nuevo Leon, FIME–Centro de Investigación e Innovación en ingeniería Aeronáutica (CIIIA), Av., Universidad s/n., Ciudad Universitaria, San Nicolás de los Garza 66455, Nuevo León, Mexico; citlalli.gaonatbr@uanl.edu.mx (C.G.-T.); marmontoya@utp.edu.co (M.M.-R.); jose.cabralmr@uanl.edu.mx (J.A.C.-M.); francisco.estupinanlp@uanl.edu.mx (F.E.-L.); patricia.zambranor@uanl.edu.mx (P.Z.-R.)

[2] Instituto de Ingeniería, Universidad Veracruzana, Boca del Río 94294, Veracruz, Mexico; rorozco@uv.mx

[3] Centro de Investigación en Materiales Avanzados (CIMAV), Miguel de Cervantes 120, Complejo Industrial Chihuahua, Chihuahua 31125, Chih, Mexico; jose.chacon@cimav.edu.mx

[4] Facultad de Ingeniería Civil-Xalapa, Universidad Veracruzana, Xalapa 91000, Veracruz, Mexico; mbaltazar@uv.mx

* Correspondence: falmeraya.uanl.ciiia@gmail.com

check for updates

Abstract: AlCrN/TiSi, AlCrN/TiCrSiN and AlCrN/AlCrN + CrN coatings were deposited on Inconel 718 alloy by physical vapour deposition (PVD). The corrosion behaviour of uncoated and coated specimens was evaluated using electrochemical impedance spectroscopy (EIS) at open circuit potential in a 3.5 wt.% NaCl and 2 wt.% H_2SO_4 solutions. The EIS data acquired were curve fitted and analysed by equivalent circuit models to calculate the pore resistance, the charge transfer resistance and the capacitance. The Nyquist diagrams of all systems showed one part of the semicircle which could relate that reaction is a one step process, except for the AlCrN/TiCrSiN and AlCrN/AlCrN + CrN coatings in H_2SO_4 solution, for which two semicircles related to active corrosion in substrate alloy were found. However, from the Bode plots, it was possible to identify two the time constants for all systems exposed to NaCl and H_2SO_4 solutions. According to electrochemical results, the corrosion resistance of the AlCrN/TiSiN coating was better in the NaCl solution, whereas the AlCrN/AlCrN + CrN coating show better performance in the Sulphuric Acid solutions.

Keywords: PVD coatings; corrosion; 718 Inconel alloy; EIS

1. Introduction

The aviation industry demands improvements in the characteristics of the structural and functional materials components of aircraft based on scientific research conducted on new materials. The intrinsic resistance of alloys alone is insufficient to protect structural components from an aggressive environment. Coatings have been applied since the 1950´s as a method of surface protection that does not have enough resistance to corrosion at high temperatures [1–3]. Initially, aluminium diffusion coatings by packing cementation on Ni-based superalloys were used [4]. These coatings provided better corrosion protection to the substrate against corrosive agents. Subsequently, other forms of coating deposition such as plasma spraying and vapour deposition techniques for high-temperature applications such as thermal barrier coatings in aircraft gas turbines were used [5]. The basic physical vapour deposition

(PVD) process fall into two general categories: sputtering and evaporation [6]. The PVD is used to deposit thin films and coatings in the solid state providing a variety of desirable surface properties such as appearance, high wear resistance, low friction and good corrosion resistance [7]. The thickness of deposits can vary from angstroms to millimeters. Very high deposition rates (25 μm/s) have been achieved with the advent of electron beam heated sources [6,8].

The Titanium nitride (TiN) is a PVD coating produced by vacuum-arc, largely employed material, which has the unique combination of physical properties. Nowadays, research activities in the field of hard coatings thrive towards the synthesis of novel multicomponent nanostructured transition metal nitride (TMN) coatings with improved ductility [9,10]. D'Avico et al. [11], mention that mould materials, nitride-coated (e.g., TiN, AlTiN and CrN) metal substrates, obtained by the Physical Vapour Deposition (PVD) method, show improved mechanical properties and good wear/corrosion resistance.

D'Avico et al. claimed that Cathodic Arc PVD process can produce very dense layers with little or no porosity, forming a single-layer or multilayer structure on the substrate [12,13]

Okumiya and Griepentrog [12,14] mention that the influence of single-layer or multilayers on mechanical and tribological properties, showing that multilayers do not seem to confer positive effects because the lifetime of the coatings is limited by the poor adhesion of the coatings on the steel substrates. On the other hand, PalDey and Deevi [15] concluded that the presence of a large number of interfaces between individual layers of a multilayered structure results an increase in strength and hardness. Kappl et al. claimed that definite improvements in the corrosion behavior of hard coatings with proper multilayer structure [12,16].

Coating systems such as TiCN, AlCN, YSZ, CrAlN, $BiMnO_3$, etc., confirm the advantages of the PVD process [17–19]. Nitrides/nitrides multilayer coatings have been studied with great interest due to their good mechanical properties and high resistance to oxidation and corrosion [20]. Also, it has been reported that TiN/CrN [21] Ti/TiN [22], Ti/CrN and Ti/TiAlN, TiAlSiN/CrAlN [23] multilayer coatings exhibit enhanced corrosion and oxidation resistance as compared to a single layer coating system.

The transition metal nitrides coatings deposited by PVD contain a columnar microstructure and high defect density, e.g., micropores, pinholes. These features might have a negative effect on the corrosion resistance of the coating system [24]. For the evaluation of corrosion behaviour of coated-metal systems, an AC measuring technique such as electrochemical impedance spectroscopy (EIS) has found wide application. This technique is to small changes in the resistive capacitive nature of the electrolyte/electrode interface, thus being effective for the study of localised corrosion via the aforementioned coating defects. [16,25,26].

Multilayer coatings had better corrosion behaviour than monolayer coatings due to the formation of a dense and compact structure reducing the number of defects such as cracks, pinholes and pores within the coatings, thereby further restricting electrolyte diffusion toward the metallic substrate. Chipatecua et al. [27] studied the corrosion behaviour of a CrN/Cr multilayer coating deposited by unbalanced magnetron sputtering (UBM) on stainless steel exposed in a NaCl solution by EIS. As a general trend, they reported that a reduction in coating thickness increases the charge transfer resistance. Due to a smaller coating thickness, the electrolyte diffusion through the coating took less time due to shorter path length, rapidly producing a dense passive low-conductivity oxide film at the bottom of permeable defects having capacitive behaviour very similar to that of ceramic coatings. Other study of CrN/Cr multilayers on H13 tool steel by EIS show that two relaxation points appeared in the phase angle vs. frequency logarithm curves, suggesting that the electrolyte penetrates through pores and pinholes of the coating and makes contact with the metallic substrate [28].

Olia et al. [29] studied the corrosion behavior of multilayers nitride coatings TiN/TiAlN and CrN/CrAlN deposited by cathodic arc PVD on 17-4 PH stainless steel. Their EIS results indicated that the martensitic steel has the lowest corrosion resistance followed by the TiN/TiAlN multilayer coating, whereas the CrN/CrAlN multilayer coating disclosed the highest corrosion resistance. Here, the CrN provide a better ability to form a passive layer on the surface; therefore, a maximum capacitive resistance was related to the CrN/CrAlN coating system, on the other hand, it is known that titanium

nitride have a columnar structure with pinholes and pores and the electrolyte lead to the substrate. For iron and steels, Grabke [30] has shown the beneficial effect of N against localized corrosion i.e., the presence of nitrides ion may inhibit pit initiation by suppressing chlorides ion.

From the above, it can be seen that there are a good body of research about the corrosion behaviour of multilayer coatings by PVD techniques deposited on metallic substrates from mild steel, stainless steel (304SS and 17-4PH), tool steels and Ti alloys. However, none has involved AlCrN/TiSiN, AlCrN/TiCrSiN and AlCrN/AlCrN + CrN PVD multilayer coatings on Inconel 718 alloy corrosive behavior.

The advanced coating materials used for wear resistance, have proven themselves to be effective hard barriers for resisting wear of the substrate metal/metal alloys. These coating varies from cobalt boride, hard diamond-like carbide (DLC) coatings, boron nitride composites, chromium nitride, aluminium trioxide, aluminium–chromium nitride, nickel chromium–chromium trioxide, zirconium dioxide [31–34]

Srinatah and Ganesha, comment that the literature have shown that both wear and corrosion resistance can be achieved through coatings and selective heat treatments of metals/metal alloys. The Studies of Wear and corrosion resistance of titanium carbo-nitride coated Al-7075 produced through PVD to characterize the bonding, using a potentiodynamic test and electrochemical impedance spectroscopy. The results of both the wear and the corrosion performance investigations were in good agreement with each other. Thus, the tribo-corrosive deterioration of titanium carbo-nitride coated Al-7075 had escalated with an increase in durations of the heat treatment [34].

The aim of this work was to study the corrosion behavior of multilayered coatings (AlCrN/TiSiN, AlCrN/TiCrSiN and AlCrN/AlCrN + CrN) deposited by PVD on Inconel 718. The electrochemical properties of the coatings have been studied using electrochemical impedance spectroscopy in two solutions: 3.5 wt.% NaCl and 2 wt.% H_2SO_4. This coating system on this superalloy might find potential applications in temperature sensors from the brake systems an aircraft.

2. Materials and Methods

2.1. Substrate Material

Nickel-base alloy Inconel 718 (0.08 C max, 17-21 Cr, 50–55 Ni, 4.75–5.50 Nb, 2.80–3.30 Mo, 0.65–1.15.Ti, 0.20–0.80 Al, 1.0 max Co, 0.35 max Mn, 0.35 max Si, 0.015 max P, 0.30 max Cu, 0.015 max S, 0.006 max B and balanced Fe in wt.%) was used as a substrate material. Before coating deposition, all substrates were ultrasonically cleaned first in an alkaline solution heated to 333 K and later in ethanol, each one for 5 min.

2.2. PVD Coating Deposition

The nitride AlCrN/TiSiN, AlCrN/TiCrSiN and AlCrN/AlCrN + CrN coatings were deposited by cathodic arc plasma assisted physical vapour deposition (PVD) using an Al 70%–Cr 30% target with nitrogen gas (N_2) ware used to obtain AlCrN coatings at 450 °C. Subsequently, TiSi, TiCrSi and Cr targets were used at 350 °C. The deposition were: (i) 60 min for AlCrN layer and (ii) 20 min for TiSiN, TiCrN and AlCrN + CrN layers. The Ar and N_2 flow were independently controlled using a mass flow controller [Fox Thermal, CA, USA], (approximately 20 and 10 sccm, standard cubic centimetres per minute). The Vacuum chamber [Oerlikon, Balzers, Leichtenstein] (10^{-5} mbar), DC-substrate bias voltage was in the range of −40 to −150 (V). The cathode current (A) was 60 A and total gas pressure was 1.5 (Pa). Table 1 shows the classification of the different PVD coatings used.

Table 1. Sample classification.

Samples	Coating
SU	Inconel 718
C1	AlCrN/TiSiN
C2	AlCrN/TiCrSiN
C3	AlCrN/AlCrN + CrN

2.3. Microstructural Characterization

Scanning Electron Microscopy (SEM, Jeol JSM 6510LV, Tokyo, Japan) was as well utilized for identifying the cross-sectional micrographs of PVD coatings a magnification of 2000X, operating at 20 kV, WD = 10 mm. The chemical composition of these multilayered structures was obtained by Energy Dispersive X-ray Spectroscopy (EDS, EDAX, Tokyo, Japan).

2.4. Electrochemical Technique

Electrochemical impedance spectroscopy (EIS) tests on uncoated and coated samples were carried out at 25 °C at the corrosion potential using a Gill-AC potentiostat/galvanostat/ZRA from ACM Instruments (Manchester, UK). Tests were performed in a conventional three-electrode cell where: the specimen (uncoated and coated, 1.0 cm^2 exposed area) was connected to a working electrode; reference and auxiliary electrodes were saturated calomel (SCE) and platinum wire, respectively. The two electrolytes were used: 3.5 wt.% NaCl and 2 wt.% H_2SO_4. After the corrosion potential stabilized, a sinusoidal a. c. signal of amplitude 10 mV (root mean square，rms) was applied coupled with the corrosion potential over a frequency range from 10 kHz to 1.0 mHz obtaining 10 points per decade according to the ASTM G106-15 standard [35]. The experimental results were interpreted through the development of typical impedance models for the electrode surfaces, and curve fitting based on equivalent circuits (using the Zview impedance program).

3. Results

3.1. Morphological Analysis

SEM/EDS cross-sectional analysis of the AlCrN/TiSiN (C1 coating) show strong peak signals for Ti, Al, Si and N at the top of the coating, whilst a strong signal for Al, Cr, and N near the coating/substrate interface was detected, indicating that the coating is mainly formed by TiAlN at the top and AlCrN near the metallic substrate see (Figure 1a)
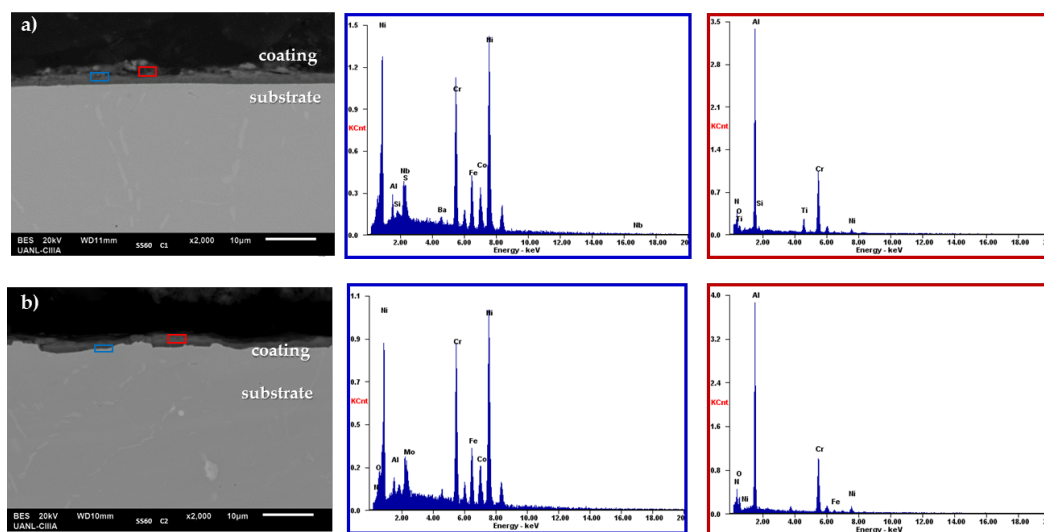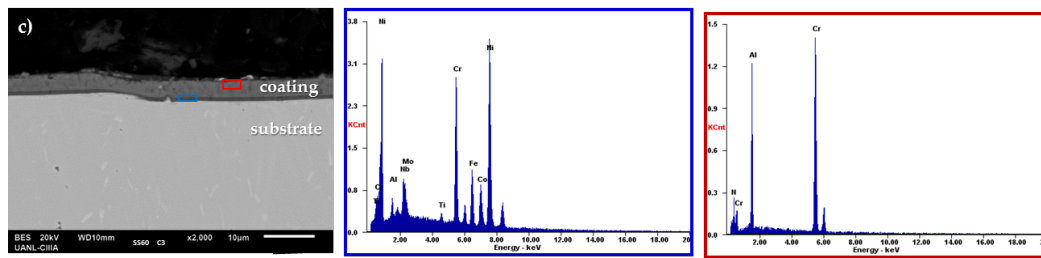

Figure 1. *Cont.*

Figure 1. SEM cross-sectional micrographs of PVD coatings and its EDS: (**a**) PVD AlCrN/TiCrSiN C1, (**b**) PVD AlCrN/CrTiSiN C2 and (**c**) PVD AlCrN/AlCrN + CrN C3 coatings.

Figure 1b presents a cross-section view of the C2 coating. The EDS spectra indicates the presence of Ti, Cr, Si, N, Co and Al (from the coating) and also the presence of Fe and Ni (from the substrate). For the C3 coating, Figure 1c shows a homogeneous coating. Strong EDS signals for Cr, Al and N where detected at the top of the coating, whilst near the coating/substrate interface, Al, Cr, N and Ni were detected (Ni comes from the metal substrate). The coating thickness for C1 and C2 was about 2 µm on each case, while the C3 coating had a thickness of about 4 µm

3.2. Corrosion Behaviour of PVD Coatings and Substrate

Figure 2 shows the Nyquist diagrams for Inconel 718 and AlCrN/TiSi (C1), AlCrN/TiCrSiN (C2) and AlCrN/AlCrN + CrN (C3) coatings exposed to 3.5 wt.% NaCl solution. For all systems, the Nyquist diagrams in Figure 2, show incomplete semi-circles, being this behaviour associated with high impedance values [36–38].
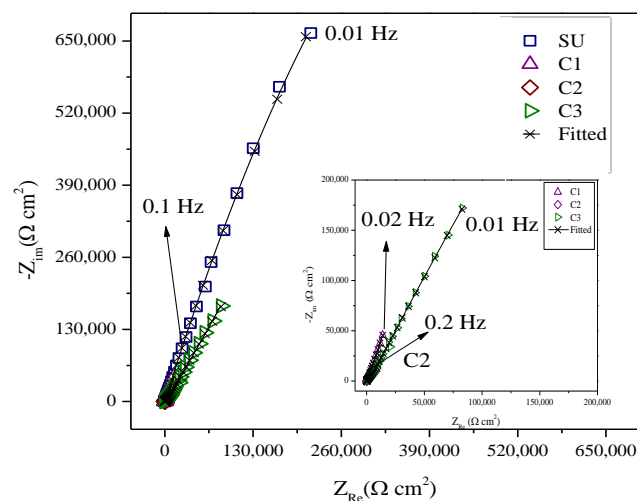

Figure 2. Nyquist diagram of substrate Inconel 718 and C1, C2 and C3 coatings exposed to 3.5 wt.% NaCl solution.

Only one semi-circle was shown for substrate SU alloy and AlCrN/TiSiN (C1) coating which are incomplete due to high impedance values when was tested in H_2SO_4 solution (Figure 3). However, for the AlCrN/TiCrSiN (C2) and AlCrN/AlCrN + CrN (C3) coatings, the Nyquist plot show flattening of their semicircles under exposure to 2 wt.% H_2SO_4 solution. In this case, the smaller semi-circle (high frequency) can be related to the coatings capacitance whilst the lower frequency semi-circle is related to the double layer capacitance. This likely indicates initiation of corrosion of the substrate alloy, and subsequently a major coating damage is expected as the electrolyte penetrates the PVD coatings [39].
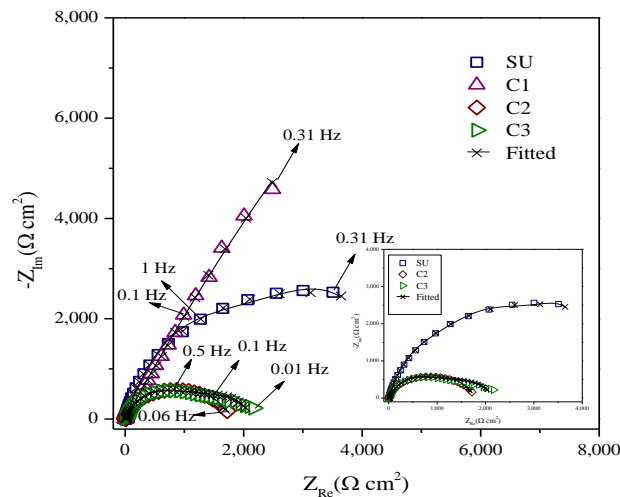
Figure 3. Nyquist diagram of substrate Inconel 718 and C1, C2 and C3 coatings exposed to 2 wt.% H_2SO_4 solution.

4. Discussion

The electrochemical results obtained show a variation between impedance measurements and the AC polarization from the different coatings and metallic substrate.A quantitative analysis of EIS was performed using two different equivalent circuit models for the different systems in the present work, Figure 4.

Figure 4. Equivalent electrical circuit models for: (**a**) one-time constant for uncoated alloy, (**b**) two-time constants for C1, C2 and C3 PVD coatings in NaCl and H_2SO_4 solutions.

The capacitive behavior exhibited for the SU substrate in NaCl solution suggests that formation of a highly stable film at pores is also capacitive. It has been reported that a dense and stable Cr_2O_3 oxide film layer is responsible of the passive behavior observed for the 718 alloy exposed in the 3.5 wt.% NaCl solution [24]. The EIS behaviour for the PVD coatings, can be related to two electrochemical process, i.e., two kinetic phenomena in each sub-interface—electrolyte/coating and electrolyte/substrate [40]. This corrosion mechanism may be related to a decrease in defect resistance as the electrolyte solution penetrates through the C1, C2 and C3 coatings and creates a diffusion path towards the base metal. It has been mentioned that galvanic corrosion may take place due to the fact that hard coatings are generally more noble than the metal [41]. The Nyquist plot of mono and multilayered CrAlN and CrAlN/SiN$_x$ coatings on 420 SS exposed in 3.5 wt.% NaCl solution, revealed a single semicircle for all samples, which was associated with insufficient exposure time in order to start the corrosion in the substrate alloy. The CrAlN coating show pitting corrosion resulting from the coating defects existing within the coating. The multilayered coatings had better corrosion protection than the single-layered one [42,43].

These figures also show the fitting data of the EEC model (see Figures 3 and 4 upper part), which matches well with the experimental data shown as individual points. The agreement of the data and the low χ^2 values corroborate the accuracy of the proposed EEC model.

The distributed electrical parameter, the constant phase element (CPE) is defined by Equation (1):

$$Z_{CPE(\omega)} = \left[\left(Y_p \right)^{-1} (j\omega)^{-n} \right] \tag{1}$$

where Y_p is the admittance, $j^2 = (-1)$, ω is the angular frequency (rad/s), and the dimensionless n ($-1 < n < 1$) is the power of the CPE [44]. The value of Y_p is of the order of the double-layer capacitance ($10-100$ µF/cm^2) typical of a charge transfer process [45].

The electrical equivalent circuit model proposed in Figure 4b, the constant phase elements CPE_c and CPE_s which represent the pseudo-capacitances at the solution/coating and coating/substrate interfaces and their empirical exponent n_1 *and* n_{dl} respectively, are listed in Table 2. Also, Table 2 shows the resistance R_e which represents the ionic solution resistance between the working electrode and reference electrode, pore resistance R_{pore} which relate the resistance of ion-conducting paths the develop the coating and transfer resistance at the coating/substrate interface R_s for uncoated alloy and PVD coatings. The CPE element represents a non-ideal capacitor according to the n value and its capacity is determined by faradaic and adsorption charging at the double layer. The n value is related to surface homogeneities ($n = 1$ for a pure capacitor, $n = 0$ for pure a resistor and $n = 0.5$ for a Warburg impedance (diffusion)) [22]. Given the fact that the n_1 value for the C3 coating was higher than that of the C1 and C2 coatings, the C3 coating had a less active behaviour in the 3.5 wt.% NaCl solution. However, once the electrolyte reaches the substrate, the system shows a resistive behavior. For this reason, two inflection points appeared in the frequency range studied in the phase angle vs frequency plot, suggesting the involvement of mass transfer through pores. Similar case occurs for the C2 coating which had high susceptibly to corrosion the coating/substrate interface. On the other hand, the n_1 value for the C1 coating was lower than its corresponding n_{dl} value.

Table 2. EIS data obtained by equivalent circuit simulation of coated and uncoated specimens exposed in 3.5 wt.% NaCl solution.

Sample	EIS Parameters								
	CPE_c (F cm^{-2})	n_1	CPE_s (F cm^{-2})	n_{dl}	R_e (Ω cm^2)	R_{pore} (Ω cm^2)	R_s (Ω cm^2)	E_{rror} %	χ^2
SU	0.000014	0.857	-	-	12.28	6,100,000	-	<16.10	0.0036
C1	0.000086	0.805	0.000030	0.88	13.17	11,000	7,940,000	<2.73	0.00061
C2	0.000024	0.774	0.000036	0.545	12.28	3200	763,000	<5.91	0.000084
C3	0.000017	0.826	0.000023	0.696	12.35	10,000	9,220,000	<4.19	0.00059

Electrical equivalent circuits for PVD coatings has been reported widely to fit the electrochemical impedance data [29,46–52]. An EIS study on CrAlSi$_x$N nitride coatings on 420 SS substrate revealed important improvements in charge-transferred resistance (R_s) and n values with increasing Si content. These improvements were associated to a dense microstructure of the CrAlSi$_x$N coatings [53]. Another EIS study of TiN and Ti–Si–N coatings on 304 SS reported the corrosion improvement when Si was added to the TiN. For TiN alone, the presence of holes provides a diffusion path for the electrolyte eventually reaching the coating/substrate interface. For the Ti–Si–N coatings, their microstructure provides longer diffusion paths. When localized corrosion occurs, the corrosion products block the diffusion path and hinder the penetration of the electrolyte, which will improve the R_{ct} value in the Ti–Si–N coating [48]. According to the above mentioned, this could relate to why the PVD AlCrN/TiSiN C1 coating obtained values of n_2 of 0.880 and R_{pore} of 11323 Ω cm^2.

The corrosion behaviors of TiN/TiAlN multilayer coatings in 3.5 wt.% NaCl solution was reported [50]. In this study, the plots show two time-constants are representing the capacitive response of double layer and coatings. Values between 10,300 and 61,800 Ω cm^2 for R_s were measured according the number of layers as of coating. In the present work for PVD C1, C2 and C3 coatings, the R_s was 7,940,000, 763,000 and 9,220,000 Ω cm^2, respectively. It is possible to relate that increased layered interfaces and high structural density can improve corrosion resistance as reported [51].

The total polarization resistance defined by $R_p = R_{pore} + R_s$ can be considered as an indicator of the corrosion resistance of the material. The R_p represents the dielectric properties of coatings and passive substrate in pores which is inversely proportional to the corrosion rate [27,28,51–54]. R_p values around 3000 and 800 kΩ for multilayer Cr/CrN/CrAlN coatings immersed in 3.0 wt.% NaCl has been reported, indicating high corrosion resistance [54]. In the present work, R_p values for the C1, C2 and C3 coating systems were 7950, 766 and 9230 kΩ cm^2, respectively.

From the Nyquist plots obtained for the substrate alloy (SU) exposed in the 2 wt.% H_2SO_4 solution, an equivalent circuit is proposed in Figure 4a, indicating the presence of a single layer (capacitance behavior) were R_e is the solution resistance, R is the passive film resistance and CPE_1 the constant-phase element characteristic for a passive film [55,56]. For the coated specimens the EIS data were fitted by a two-time constants equivalent circuit, Figure 4b, and the parameters for this equivalent circuit are shown in Table 3.

Table 3. EIS data obtained by equivalent circuit obtained simulation of coated and uncoated specimens exposed in 2 wt.% H_2SO_4 solution.

Sample	EIS Parameters								
	CPE_c (F cm^{-2})	n_1	CPE_2 (F cm^{-2})	n_{dl}	R_e (Ω cm^2)	R_{pore} (Ω cm^2)	R_s (Ω cm^2)	E_{rror} %	χ^2
SU	0.000069	0.894	-	-	7.205	5968	-	<0.56	0.00021
C1	0.00036	0.891	0.00036	0.75	7.292	1347	36377	<3.08	0.00025
C2	0.000091	0.876	0.00075	0.851	7.976	1240	511.3	<2.33	0.00067
C3	0.00020	0.849	0.0038	0.842	9.242	1428	704.7	<1.84	0.00083

It is important to mention that R_s and double layer capacitance (CPE_{-s}) are dependent on the affected area of the substrate. As the area increases, R_s decreases, and the reverse is true for CPE_{-s}. Due to this, the H_2SO_4 electrolyte resistance is the lowest compared to the NaCl solution, thus, greater corrosion is often uncoated specimens could be expected under exposure to the H_2SO_4 solution at the metal surface.

5. Conclusions

The PVD AlCrN/TiSiN and AlCrN/TiCrSiN coatings did not present a homogeneous and compact bonding with the bottom layer and substrate. It could have been due that atoms of the top layer did not diffuse into the bottom layer and substrate, respectively.

The EIS measurements of uncoated substrate showed the presence of a single time constant. However, the corrosion mechanism for all PVD coatings was determined by an equivalent circuit containing two-time constants, which described two electrochemical process in the electrolyte/coating and coating/substrate interfaces.

The corrosion resistance of the AlCrN/TiSiN coating was better in the sodium chloride solution, whereas the AlCrN/AlCrN + CrN coating show better performance in the Sulphuric Acid solution. In both cases they had, the lowest corrosion current density, highest protective efficiency and largest charge transfer resistance than that of other bilayer.

PVD technology is becoming an emerging alternative for the aeronautical industry to produce hard coatings with applications in temperature sensors from the brake system of an aircraft.

Author Contributions: Conceptualization F.A.-C., C.G.-T. and M.M.-R.; Methodology, J.A.C.-M., P.Z.-R., C.G.-T., R.O.C. and F.E.-L.; Data Curation, C.G.-T., M.Á.B.-Z., J.A.C.-M., and M.M.-R.; Writing—Review and Editing, F.A.-C., J.G.C.-N. and M.M.-R. All authors have read and agreed to the published version of the manuscript.

Conflicts of Interest: The authors declare no conflict of interest.

References

1. Tiong, U.H.; Clark, G. The structural environment as a factor affecting coating failure in aircraft joints. *Procedia Eng.* **2010**, *2*, 1393–1401. [CrossRef]

2. Clark, G. Corrosion and the management of structural integrity. In *ICAF'99:Structural Integrity for the Next Millennium*; Rudd, J.L., Ed.; EMAS Ltd.: Warley, UK, 1999.

3. Trinstancho-Reyes, J.L.; Sanchez-Carrillo, M.; Sandoval-Jabalera, R.; Orozco-Carmona, V.M.; Almeraya-Calderon, F.; Chacon-Nava, J.G.; Gonzalez-Rodriguez, J.G.; Martinez-Villafane, A. Electrochemical impedance spectroscopy investigation of alloy Inconel 718 in molten salts at high temperature. *J. Electrochem. Sci.* **2011**, *6*, 419–431.

4. Bianco, R.; Rapp, R.A. Pack cementation diffusion coatings. In *Metallurgical and Ceramic Protective Coatings*; Springer: Dordrecht, The Netherlands, 1996; pp. 236–260.

5. Zhang, S.; Zhao, D. (Eds.) *Aerospace Materials Handbook*; CRC Press: Boca Raton, FL, USA, 2013.

6. Mubarak, A.M.A.; Hamzah, E.H.E.; Toff, M.T.M. Review of Physical vapour depositetion (PVD) techinques for hard coating. *J. Mek.* **2005**, *20*, 42–51.

7. Savisalo, T.; Lewis, D.; Luo, Q.; Bolton, M.; Hovsepian, P. Structure of duplex CrN/NbN coatings and their performance against corrosion and wear. *Surf. Coat. Technol.* **2008**, *202*, 1661–1667. [CrossRef]

8. Bunshah, R.F.; Deshpandey, C.V. Hard coatings. *Vacuum* **1998**, *30*, 955–965.

9. Kalinichenko, A.I.; Reshetnyak, E.; Strel'nitskij, V.; Abadias, G. Role of nonlocal thermoelastic peaks in the stress and texture evolution of TiN coatings formed by plasma based ion implantation and deposition. *Surf. Coat. Technol.* **2020**, *391*, 12565. [CrossRef]

10. Cavaleiro, A.; de Hosson, J.T. (Eds.) *Nanostructured Coatings*; Springer: New York, NY, USA, 2006.

11. D'Avico, L.; Beltrami, R.; Pargoletti, E.; Trasatti, S.P.; Cappelletti, G. Insight into the release agents/PVD coatings interaction for plastic mold technology. *Coatings* **2020**, *10*, 281. [CrossRef]

12. D'Avico, L.; Beltrami, R.; Lecis, N.; Trasatti, S.P. Corrosion behavior and surface properties of PVD coatings for mold technology applications. *Coatings* **2018**, *9*, 7. [CrossRef]

13. Yoon, S.-Y.; Kim, J.-K.; Kim, K.H. A comparative study on tribological behavior of TiN and TiAlN coatings prepared by arc ion plating technique. *Surf. Coat. Technol.* **2002**, *161*, 237–242. [CrossRef]

14. Okumiya, M.; Griepentrog, M. Mechanical properties and tribological behavior of TiN–CrAlN and CrN–CrAlN multilayer coatings. *Surf. Coat. Technol.* **1999**, *112*, 123–128. [CrossRef]

15. PalDey, S.; Deevi, S. Single layer and multilayer wear resistant coatings of (Ti,Al)N: A review. *Mater. Sci. Eng. A* **2003**, *342*, 58–79. [CrossRef]

16. Fenker, M.; Balzer, M.; Kappl, H. Corrosion protection with hard coatings on steel: Past approaches and current research efforts. *Surf. Coat. Technol.* **2014**, *257*, 182–205. [CrossRef]

17. Caicedo, J.; Amaya, C.; Yate, L.; Aperador, W.; Zambrano, G.; Gomez, M.-E.; Alvarado-Rivera, J.; Muñoz-Saldaña, J.; Prieto, P. Effect of applied bias voltage on corrosion-resistance for $TiC_{1-x}N_x$ and $Ti_{1-x}Nb_xC_{1-y}N_y$ coatings. *Appl. Surf. Sci.* **2010**, *256*, 2876–2883. [CrossRef]

18. Yate, L.; Caicedo, J.C.; Macias, A.H.; Espinoza-Beltrán, F.J.; Zambrano, G.; Muñoz-Saldaña, J.; Prieto, P. Composition and mechanical properties of AlC, AlN and AlCN thin films obtained by rf magnetron sputtering. *Surf. Coat. Technol.* **2009**, *203*, 1904–1907. [CrossRef]

19. Amaya, C.; Aperador, W.; Caicedo, J.C.; Espinoza-Beltrán, F.J.; Muñoz-Saldaña, J.; Zambrano, G.; Prieto, P. Corrosion study of alumina/yttria-stabilized zirconia (Al2O3/YSZ) nanostructured thermal barrier coatings (TBC) exposed to high temperature treatment. *Corros. Sci.* **2009**, *51*, 2994–2999. [CrossRef]

20. Nordin, M.; Larsson, M.; Hogmark, S. Mechanical and tribological properties of multilayered PVD TiN/CrN, TiN/MoN, TiN/NbN and TiN/TaN coatings on cemented carbide. *Surf. Coat. Technol.* **1998**, *106*, 234–241. [CrossRef]

21. Nordin, M.; Larsson, M.; Hogmark, S. Mechanical and tribological properties of multilayered PVD TiN/CrN. *Wear* **1999**, *232*, 221–225. [CrossRef]

22. Ries, L.; Azambuja, D.; Baumvol, I. Corrosion resistance of steel coated with Ti/TiN multilayers. *Surf. Coat. Technol.* **1997**, *89*, 114–120. [CrossRef]

23. Dobrzański, L.A.; Lukaszkowicz, K.; Kriz, A. Properties of the multi-layer Ti/CrN and Ti/TiAlN coatings deposited with the PVD technique onto the brass substrate. *J. Mater. Process. Technol.* **2003**, *143*, 832–837. [CrossRef]

24. Barshilia, H.C.; Rajam, K. Structure and properties of reactive DC magnetron sputtered TiN/NbN hard superlattices. *Surf. Coat. Technol.* **2004**, *183*, 174–183. [CrossRef]

25. Oliveira, V.; Aguiar, C.; Vázquez, A.; Robin, A.; Barboza, M. Improving corrosion resistance of Ti–6Al–4V alloy through plasma-assisted PVD deposited nitride coatings. *Corros. Sci.* **2014**, *88*, 317–327. [CrossRef]

26. Liu, C.; Bi, Q.; Matthews, A. EIS comparison on corrosion performance of PVD TiN and CrN coated mild steel in 0.5 N NaCl aqueous solution. *Corros. Sci.* **2001**, *43*, 1953–1961. [CrossRef]

27. Chipatecua, Y.; Olaya, J.; Arias, D.F. Corrosion behaviour of CrN/Cr multilayers on stainless steel deposited by unbalanced magnetron sputtering. *Vacuum* **2012**, *86*, 1393–1401. [CrossRef]

28. Marulanda, D.; Olaya, J.; Piratoba, U.; Marino, A.; Camps, E. The effect of bilayer period and degree of unbalancing on magnetron sputtered Cr/CrN nano-multilayer wear and corrosion. *Thin Solid Films* **2011**, *519*, 1886–1893. [CrossRef]

29. Olia, H.; Ebrahimi-Kahrizsangi, R.; Ashrafizadeh, F.; Ebrahimzadeh, I. Corrosion study of TiN, TiAlN and CrN multilayer coatings deposit on martensitic stainless steel by arc cathodic physical vapour deposition. *Mater. Res. Express* **2019**, *6*, 046425. [CrossRef]

30. Grabke, H.J. High Nitrogen Steels. The Role of nitrogen in the corrosion of iron and steels. *ISIJ Int.* **1996**, *36*, 777–786. [CrossRef]

31. Li, Z.; Di, S. The Microstructure and wear resistance of microarc oxidation composite coatings containing nano-hexagonal boron nitride (HBN) particles. *J. Mater. Eng. Perform.* **2017**, *26*, 1551–1561. [CrossRef]

32. Wang, L.; Nie, X. Effect of annealing temperature on tribological properties and material transfer phenomena of CrN and CrAlN coatings. *J. Mater. Eng. Perform.* **2013**, *23*, 560–571. [CrossRef]

33. Hong, L.; Bian, G.; Hu, S.; Wang, L.; Dacosta, H. Tribological properties of CrAlN and TiN coatings tested in nano- and micro-scale laboratory wear tests. *J. Mater. Eng. Perform.* **2015**, *24*, 2670–2677. [CrossRef]

34. Srinath, M.K.; Prasad, M.S.G. Wear and corrosion resistance of titanium carbo-nitride coated Al-7075 produced through PVD. *Bull. Mater. Sci.* **2020**, *43*, 1–11. [CrossRef]

35. ASTM G106-15. *Standard Practice for Verification of Algorithm and Equip for Electrochemical Impedance Measurements*; ASTM: West Conshohocken, PA, USA, 2015.

36. Taberna, P.L.; Simon, P.; Fauvarque, J.F. Electrochemical characteristics and impedance spectroscopy studies of carbon-carbon supercapacitors. *J. Electrochem. Soc.* **2003**, *150*, A292–A300. [CrossRef]

37. Wang, Y.; Northwood, D. An investigation of the electrochemical properties of PVD TiN-coated SS410 in simulated PEM fuel cell environments. *Int. J. Hydrogen Energy* **2007**, *32*, 895–902. [CrossRef]

38. Moisel, M.; De Mele, M.A.F.L.; Müller, W.-D.; De Mele, M.F.L. Biomaterial interface investigated by electrochemical impedance spectroscopy. *Adv. Eng. Mater.* **2008**, *10*, B33–B46. [CrossRef]

39. Chen, T.; Nutter, J.; Hawk, J.; Liu, X. Corrosion fatigue crack growth behavior of oil-grade nickel-base alloy 718. Part 1: Effect of corrosive environment. *Corros. Sci.* **2014**, *89*, 146–153. [CrossRef]

40. Grips, V.W.; Barshilia, H.C.; Selvi, V.E.; Rajam, K. Electrochemical behavior of single layer CrN, TiN, TiAlN coatings and nanolayered TiAlN/CrN multilayer coatings prepared by reactive direct current magnetron sputtering. *Thin Solid Films* **2006**, *514*, 204–211. [CrossRef]

41. Jehn, H. Improvement of the corrosion resistance of PVD hard coating–substrate systems. *Surf. Coat. Technol.* **2000**, *125*, 212–217. [CrossRef]

42. Tsai, S.H.; Duh, J.-G. Microstructure and corrosion properties of multilayered CrAlN/SiN$_x$ coatings. *J. Electrochem. Soc.* **2010**, *157*, K89. [CrossRef]

43. Liu, C.; Bi, Q.; Leyland, A.; Matthews, A. An electrochemical impedance spectroscopy study of the corrosion behaviour of PVD coated steels in 0.5 N NaCl aqueous solution: Part I. Establishment of equivalent circuits for EIS data modelling. *Corros. Sci.* **2003**, *45*, 1243–1256. [CrossRef]

44. Manohar, A.K.; Bretschger, O.; Nealson, K.H.; Mansfeld, F. The use of electrochemical impedance spectroscopy (EIS) in the evaluation of the electrochemical properties of a microbial fuel cell. *Bioelectrochemistry* **2008**, *72*, 149–154. [CrossRef]

45. Miranda, D.A.; Jaimes, S.A.; Bastidas, J.M. Assessment of carbon steel microbiologically induced corrosion by electrical impedance spectroscopy. *J. Solid State Electrochem.* **2014**, *18*, 389–398. [CrossRef]

46. Liu, C.; Bi, Q.; Leyland, A.; Matthews, A. An electrochemical impedance spectroscopy study of the corrosion behaviour of PVD coated steels in 0.5 N NaCl aqueous solution: Part II.: EIS interpretation of corrosion behaviour. *Corros. Sci.* **2003**, *45*, 1257–1273. [CrossRef]

47. Lin, C.; Duh, J.-G. Electrochemical impedance spectroscopy (EIS) study on corrosion performance of CrAlSiN coated steels in 3.5 wt.% NaCl solution. *Surf. Coat. Technol.* **2009**, *204*, 784–787. [CrossRef]

48. Wan, Q.; Ding, H.; Yousaf, M.; Chen, Y.; Liu, H.; Hu, L.; Yang, B. Corrosion behaviors of TiN and Ti–Si–N (with 2.9 at.% and 5.0 at.% Si) coatings by electrochemical impedance spectroscopy. *Thin Solid Films* **2016**, *616*, 601–607. [CrossRef]

49. Er, D.; Azar, G.T.P.; Kazmanli, M.; Ürgen, M. The corrosion protection ability of TiAlN coatings produced with CA-PVD under superimposed pulse bias. *Surf. Coat. Technol.* **2018**, *346*, 1–8. [CrossRef]

50. Zhang, L.; Chen, Y.; Feng, Y.; Chen, S.; Wan, Q.-L.; Zhu, J.-F. Electrochemical characterization of AlTiN, AlCrN and AlCrSiWN coatings. *Int. J. Refract. Met. Hard Mater.* **2015**, *53*, 68–73. [CrossRef]

51. Li, G.; Zhang, L.; Cai, F.; Yang, Y.; Wang, Q.; Zhang, S. Characterization and corrosion behaviors of TiN/TiAlN multilayer coatings by ion source enhanced hybrid arc ion plating. *Surf. Coat. Technol.* **2019**, *366*, 355–365. [CrossRef]

52. Ruden, A.; Parra, E.R.; Paladines, A.; Sequeda, F. Corrosion resistance of CrN thin films produced by DC magnetron sputtering. *Appl. Surf. Sci.* **2013**, *270*, 150–156. [CrossRef]

53. Vasilescu, E.; Drob, P.; Vasilescu, E.; Demetrescu, I.; Ionita, D.; Prodana, M.; Drob, S.I. Characterisation and corrosion resistance of the electrodeposited hydroxyapatite and bovine serum albumin/hydroxyapatite films on Ti–6Al–4V–1Zr alloy surface. *Corros. Sci.* **2011**, *53*, 992–999. [CrossRef]

54. Lee, J.H.; Ahn, S.H.; Kim, J.G. Effect of Al additions in WC-$(Cr_{1-x}Al_x)$N coatings on the corrosion resistance of coated AISI D2 steel in a deaerated 3.5 wt.% NaCl solution. *Surf. Coat. Technol.* **2005**, *190*, 417–427. [CrossRef]

55. Almeraya-Calderón, F.; Montoya, R.M.; Garza Montes de Oca, N.; Castorena, G.J.H.; Estupiñan, L.F.; Cabral, M.J.; Maldonado, B.E.; Gaona-Tiburcio, C. Corrosion behavior of multilayer coatings deposited by PVD on Inconel 718 in Chloride and Sulphuric Acid solutions. *J. Electrochem. Sci.* **2019**, *14*, 9596–9609. [CrossRef]

56. Amin, M.A.; El-Bagoury, N.; Saracoglu, M.; Ramadan, M. Electrochemical and corrosion behavior of cast Re-containing Inconel 718 alloys in Sulphuric Acid solutions and the effect of Cl. *Int. J. Electrochem. Sci.* **2014**, *9*, 5352–5374.